

Article

Effects of Urbanization on Watershed Evapotranspiration and Its Components in Southern China

Qingzhou Zheng ¹, Lu Hao ^{1,*}, Xiaolin Huang ¹, Lei Sun ² and Ge Sun ³

¹ Key Laboratory of Meteorological Disaster, Ministry of Education (KLME)/Jiangsu Key Laboratory of Agricultural Meteorology, Nanjing University of Information Science & Technology, Nanjing 210044, China; zhengqz@nuist.edu.cn (Q.Z.); hxl@sunny0302@163.com (X.H.)

² Yangzhong Meteorological Bureau, Zhenjiang 212200, China; sl_nuist@163.com

³ Eastern Forest Environmental Threat Assessment Center, Southern Research Station, USDA Forest Service, Research Triangle Park, NC 27709, USA; ge.sun@usda.gov

* Correspondence: haolu@nuist.edu.cn

Received: 21 January 2020; Accepted: 26 February 2020; Published: 28 February 2020



Abstract: Understanding the effects of land use change on evapotranspiration (ET) and its partitioning to transpiration and evaporation is important for accurately evaluating the likely environmental impacts on watershed water supply, climate moderation, and other ecosystem services (e.g., carbon sequestration and biodiversity). This study used a distributed hydrologic model, MIKE SHE, to partition evapotranspiration into soil evaporation, transpiration, ponded water evaporation, and interception, and examined how the ET partitions affected the water balance in the Qinhuai River Basin from 2000 to 2013. Simulated daily ET was compared to measurements at an eddy flux research site during 2016–2017 ($R^2 = 0.72$). Degradation in rice-wheat rotation fields and expansion of impervious surfaces impacted not only total watershed evapotranspiration, which showed a significant downward trend ($p < 0.05$), but also its partitioning. A significant ($p < 0.01$) decrease in transpiration was detected. Ponded water evaporation was the only ET partition that exhibited a significant positive trend ($p < 0.05$). We concluded that the reduced transpiration as a result of land use and land cover change was the primary factor driving the variation of watershed scale evapotranspiration. In addition, there was an increase in annual water yield (23%) as a response to significant reduction in ET (7%) due to a 175% expansion of urban area in the study watershed. Our study provided insights to the mechanisms of land surface–water cycle interaction and better understanding of the effects of land use change on urban micro-climate such as “urban dry island” and “urban heat island” effects.

Keywords: evapotranspiration partitioning; land use and land cover change; MIKE SHE model; urbanization; hydrological modeling

1. Introduction

Urbanization-associated land use and land cover (LULC) change is a global phenomenon that has negative impacts on local environment, society, and culture [1,2]. During the urbanization processes, entire watershed water energy and balances are altered [3–5]. The elevated peak-flow rates and exacerbated flood risks represent the most obvious direct consequences [6,7]. It is essential to understand these fundamental processes to accurately evaluate the likely environmental impacts of urbanization on watershed water supply, climate moderation, and other ecosystem services such as carbon sequestration [8,9]. In particular, evapotranspiration (ET) is a critical process that links

energy, water, and carbon cycles and is recognized as a key variable to understanding the effects of urbanization on land surface processes [10–12].

Water shortage has become more acute and is expected to continue to expand due to population rise and associated increased water demand [13]. A warming climate has further increased the need for productive and rational use of traditionally marginal water and land resources [14]. ET partition studies help improve estimating crop yield and local groundwater storage [15,16]. Thus, accurately assessing ET components has been an area of interest to hydrologists in recent years [17]. Vegetation transpiration (T), soil evaporation (E_s), canopy interception evaporation (E_i), and ponded water evaporation (E_p) are four components of terrestrial ET [18]. Vegetation transpiration has long been acknowledged to be a biological process that is closely related with ecosystem productivity, whereas evaporation (E_i , E_s , and E_p) is physically controlled processes representing evaporation from wet canopy or ground surfaces [12,19,20]. T represents the largest loss of water from vegetation and the transpiration fraction (T/ET), as an indicator of ET partition, is a key to interpreting vegetation–climate feedback [21,22], validating hydrological prediction, and improving agricultural water management practices [19]. Along with the expansion in urban land use that is well known to increase storm flow as a result of increase in impervious surface and decreased ET [2], T reduction during urbanization is likely to cause large impacts on regional ecosystem productivity and water yield, because the T process directly links plant growth and the carbon cycle [17,23]. Therefore, analyses of ET partitions are more informative than ET alone for understanding how ecosystem water cycles change in varying environments [10]. Particularly, in agricultural land, calculation of ET partitions is of great importance for water resource management practices, irrigation systems and irrigation regimes planning, and crop yield estimation [16].

Various approaches have been developed to separate ET at different time and spatial scales (Table 1), including field experiment and physical based modeling methods. These methods suggest that methods for quantifying T and E_s are well developed, but separating T and E_i or separating E_s and E_p is difficult. For example, isotopes, partitioning ET into E_s and T by fractionating the isotopic composition of water, was widely used in determining plants ET but limited by its use range and high cost [20,24,25]. With the development of remote sensing technology, a series of ecological models has emerged to partition ET [26,27]. The first “two-source model”, Shuttleworth–Wallace model, was put forward in 1985 [28] and is accurate enough for plantation management [20]. However, questions remain related to the algorithm complexity when describing key parameters such as canopy and ground resistance [29]. Another commonly used model, Dual-Kc [16], requires relatively fewer parameters, but is only applicable to well-watered underlying surfaces [30]. The applicability of the above three methods is limited and would tend to underestimate ET since they can only obtain E_s and T [20,25,29]. The Priestley–Taylor Jet Propulsion Laboratory Model (PT-JPL) takes E_i into consideration, providing a more complete picture of ET research [31]. Nevertheless, given the difficulty of obtaining high quality and cloud-free remote sensing images, the remote sensing-based methods may result in a significant degree of uncertainty [26]. Therefore, hydrological models that describe ET partitions are desirable. For example, MIKE SHE (MIKE Système Hydrologique Européen/European Hydrological System), a distributed hydrological model based on water balance, offers the possibility to partition ET into four main components, namely transpiration (T), soil evaporation (E_s), interception evaporation (E_i), and ponded water evaporation (E_p), and simultaneously to be applied to multiple spatiotemporal scales in a rapid urbanization basin [32,33].

This study selected the Qinhuai River Basin (QRB), a rice paddy-dominated watershed in the Yangtze River Delta region, to explore the response of the hydrological process to LULC change. The Yangtze River Delta is the most developed and industrialized region in China that has experienced dramatic urbanization and population growth during the last several decades [34]. Rice-wheat rotation fields have been major sources of food production for thousands of years in this region [2]. Rice paddy fields have similar ecosystem services as wetlands, including flood retention, groundwater recharge [35,36], nutrient cycling, and sequestration of greenhouse gases [37]. However, rapid

rise in urban areas by converting paddy fields inevitably led to huge alterations in the watershed hydrology [19,38–40]. Du et al. [6] quantified the effects of urbanization on flood events using the Hydrologic Engineering Center’s Hydrologic Modeling System (HEC-HMS) for the same study area and found that the stream peak-flow of eight selected floods increased from 2.3% to 13.9% when urban built-up areas increased from 3% in 1988 to 31% in 2018.

Table 1. A comparison of evapotranspiration partitioning approaches.

Approaches		Theory	Scale	Partitioning	Advantages	Disadvantages	Publication
Measurement	Isotope	Hydrogen and oxygen isotopic fractionation	Field	E_s, T	Direct measurements	Costly Limited data Complex operation	[20,25]
Model	Shuttleworth-Wallace	P-M equation	Field	E_s, T	Flexible Easy to apply	Over-parameterization Limited application condition	[20,29]
	Dual-Kc	$ET_0 \times K_C$	Field	E_s, T	Few parameters needed Simple no calculation of aerodynamic and surface resistance needed	Limited applications	[30]
	PT-JPL	Priestley-Taylor algorithm	Region	E_s, T, E_i	Accurate	Uncertainty in remote sensing data	[26,31]
	MIKE SHE	Water balance	Region	E_s, T, E_i, E_p	Accurate	Numerous input parameters	[29,32,33]

As the only common term between surface energy balance and hydrological cycle, ET is a critical process to understand the impacts of LULC change on the hydrology and local climate in the QRB [2,41–43]. However, some of these previous regional studies during the past decade focused on reference evapotranspiration rate (ET_0), which only represented the atmospheric evaporating capability of a hypothetical reference vegetated field [16]. A recent study detected opposite changing direction for annual averaged ET_0 and ET trends across the QRB [2], indicating that more attention should be paid to the ET research for the hydrological interest, although understanding ET_0 is important for quantifying the change in ET. Studies on changes in the ET components in the QRB, i.e., vegetation transpiration (T), soil evaporation (E_s), vegetation interception evaporation (E_i), and ponded water evaporation (E_p), are few and limited. How the partitions dominate the spatial and temporal variability of ET has not been adequately addressed in previous research. Research is needed to link ET and water resources for understanding ecosystem evolution, environmental dynamics and putting forward effective water resource management measures under the background of rapid urbanization for the QRB.

The main aims of our research were: (1) to identify the variations in ET and its partitions (T, E_i , E_s and E_p) with different land use types in the Qinhuai River Basin from 2000 to 2013; (2) to explore the dominant ET partitions contributing to ET changes at catchment scale; and (3) to evaluate the potential effects of land conversion on local water recycling. This research helps enhance understanding the ecohydrological responses to environmental changes in an urbanizing region, and thus assists formulating policies to protect local natural resources and environment against potential harm from rapid urbanization.

2. Methods

2.1. Study Area

The Qinhuai River Basin (31°34′–32°10′ N, 118°39′–119°19′ E) is in the Yangtze River Delta region that includes Nanjing, Lishui, and Jurong cities and has a typical subtropical monsoon climate. The mean annual precipitation is 1116 mm/year and has not changed significantly from 1986 to 2013. Over 50% annual precipitation falls from June to August. The long-term mean annual temperature is about 15.4 °C. Annual air temperature has increased 0.44 °C per decade from 1990 to 2013 [2,43]. The QRB has an area of about 2631 km² with an elevation below 300 m above sea level (Figure 1). The dominant land use is rice-wheat rotation field, which accounts for more than 35% of the total watershed area. Winter wheat and paddy rice crops grown in rotation are the most common cropping

system in the QRB [2]. Rice-wheat rotation fields require flood irrigation during the entire rice growing season from May to October [43]. However, rice-wheat rotation fields have reduced by 32.5% while urban areas expanded 1.8 times, mainly due to rapid urbanization from 2000 to 2013 (Figure 2b). About 16.5% of rice-wheat rotation fields were converted into urban spaces (Figure 2a). The main soil types are yellow-brown soil, purple soil, limestone soil, paddy soil, and gray fluvo-aquic soil [6]. The aquifer is mainly made of fine sandstone, coarse sandstone, and conglomeratic sandstone, which are generally fractured and highly permeable. The main supply source is precipitation infiltration [44].

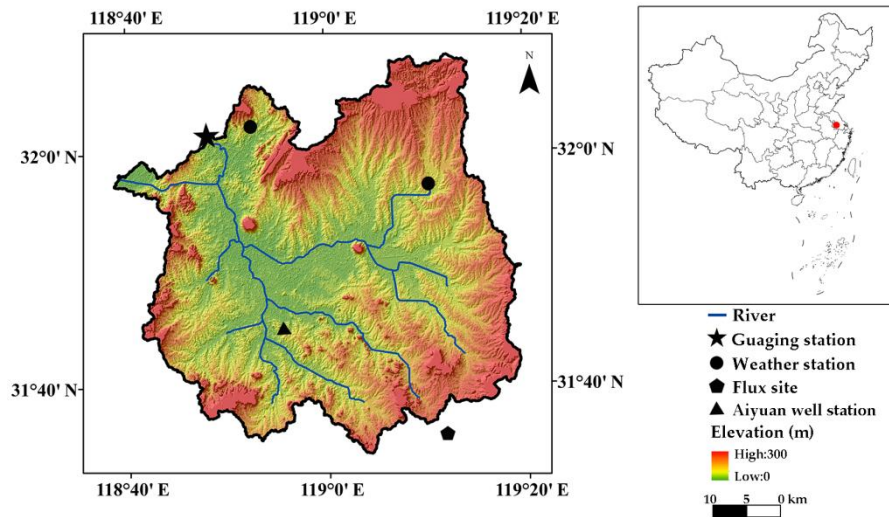


Figure 1. Digital elevation model and locations of eddy flux measurement, standard weather stations, well station, and hydrologic gauging stations measuring streamflow in the Qinhuai River Basin, southern China.

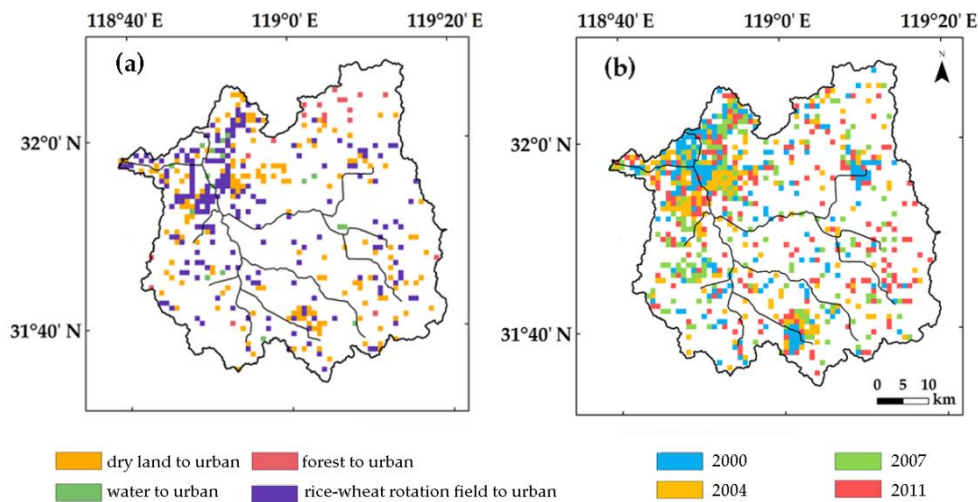


Figure 2. Land use change to urban from 2000 to 2013 (a) and urban area expansion in 2000, 2004, 2007, and 2011 (b). Each pixel has an area of 1 km².

2.2. Hydrology Model

MIKE SHE is a physically-based watershed hydrological model created by DHI (Danish Hydraulic Institute) [33]. It simulates entire hydrological processes occurring in watersheds, including streamflow, soil and groundwater dynamics, and all ET processes [45,46]. MIKE SHE is particularly useful for simulating the interactions between the unsaturated soil zone and the surficial aquifer [46,47]. Water movement in the unsaturated zone affects water exchange between the unsaturated and saturated

zones, as well as ET rates [48–50]. The one-dimensional Richards' equation was used for calculating flow in the unsaturated zone [51,52]. The ET module, based on empirical equations by Kristensen and Jensen [53], is used whenever Richards equation is used [33,53]. The ET rates are calculated as a function of reference evapotranspiration rate (ET_0), maximum plant root depth, plant leaf area index (LAI), and soil moisture content. ET is modeled by several components including: (1) evaporation from the canopy interception; (2) evaporation from the soil surface; and (3) water uptake by plant roots as transpiration modeled as a function of soil moisture in the unsaturated root zone [33]. Thus, the four main ET partitions (i.e., T , E_s , E_i , and E_p) can be estimated separately using the MIKE SHE model.

The MIKE SHE model considers the canopy as a reservoir that retains precipitation [33]. Water loss from the canopy surface is simulated by the interception evaporation process. The maximum amount of stored water, I_{max} (L), is conditional to vegetation type and growth stage as represented by the leaf area index, LAI.

Therefore,

$$I_{max} = C_{int} \times LAI \quad (1)$$

where C_{int} is an interception coefficient (L), reflecting the interception storage capacity.

$$E_i = \min (I_{max}, ET_{ref} \Delta t) \quad (2)$$

where E_i is the canopy evaporation (L/T), ET_{ref} denotes the reference evapotranspiration (L/T), and Δt is time step.

If interception storage does not satisfy the maximum amount of ET, water is evaporated from the ponded water until the ponded storage is exhausted.

$$E_p = ET_{ref} \times k_c \times \Delta t \quad (3)$$

where E_p is ponded water evaporation (L/T). k_c is crop coefficient that varies by season and crop type.

Transpiration (T) from the vegetation depends on vegetation characteristics, soil moisture content in the root zone, and root density.

$$T = f_1(LAI) \times f_2(\theta) \times RDF \times ET_{ref} \times \Delta t \quad (4)$$

$$f_1(LAI) = C_2 + C_1 LAI \quad (5)$$

$$f_2(\theta) = 1 - \left[\frac{\theta_{FC} - \theta}{\theta_{FC} - \theta_W} \right]^{\frac{C_3}{ET_{ref}}} \quad (6)$$

$$\log R(z) = \log R_0 - AROOT \times z \quad (7)$$

$$RDF = \int_{Z_1}^{Z_2} R(z) dz / \int_0^{L_R} R(z) dz \quad (8)$$

where T is actual transpiration (L/T); C_1 , C_2 , and C_3 are empirical parameters; θ_{FC} is the volumetric moisture content at field capacity; θ_W is the volumetric moisture content at the wilting point; θ_r is the residual soil moisture content; θ is the actual volumetric moisture content that varies over time; R_0 is the root extraction at the soil surface; $AROOT$ is a parameter that describes the root mass distribution (1/m); and z is the depth below ground surface (L). RDF is a root distribution function.

Soil evaporation from the upper layer of the unsaturated zone including E_s is modeled as:

$$E_s = ET_{ref} \times f_3(\theta) + (ET_{ref} - T - ET_{ref} \times f_3(\theta)) \times f_4(\theta) \times (1 - f_1(LAI)) \times \Delta t \quad (9)$$

$$f_3(\theta) = \begin{cases} C_2 & \theta \geq \theta_W \\ C_2 \frac{\theta}{\theta_W} & \theta_r \leq \theta \leq \theta_W \\ 0 & \theta \leq \theta_r \end{cases} \quad (10)$$

The hydraulic conductivity function $K(\theta)$ and the soil moisture retention curve $\theta(\varphi)$ are two hydraulic functions governing the unsaturated flow. These functions were derived from common soil properties (i.e., texture and structure) [33]. The Van Genuchten formula [54] describing soil moisture–pressure relationship was used in this study:

$$\theta(\varphi) = \theta_r + \frac{(\theta_s - \theta_r)}{\left[1 + (\alpha \cdot \varphi)^n\right]^m} \quad (11)$$

where θ_s is saturated soil moisture content; m is related to the empirical constant n by $m = 1 - \frac{1}{n}$; and α is an empirical constant. Those parameters were fitted using soil moisture release curve data.

2.3. Model Parameterization

2.3.1. Topography and Hydrogeology

Digital Elevation Model (DEM) data with a 30 m resolution (Figure 1) provided by the National Geomatics Center of China (<http://www.ngcc.cn/>) were rescaled from the original $30 \times 30 \text{ m}^2$ to $1000 \times 1000 \text{ m}^2$ (i.e., per unit area is 1 km^2). The simulation domain had about 2600 horizontal meshes that cover the entire QRB. Stream channel cross-section data were extracted from DEM data every 3 km and were used to simulate the complete terrestrial water cycle by coupling with the flow routing model, MIKE 11 [33,51]. Streamflow was computed using a fully coupled MIKE SHE/MIKE 11 model. Boundary conditions were set as zero flux at the watershed boundary.

2.3.2. Land Use and Land Cover

Land use/land cover data for four years (2000, 2004, 2007 and 2011) were derived from remote sensing products from the Geospatial Data Cloud (<http://www.gscloud.cn/>) representing four different periods (2000–2003, 2004–2006, 2007–2010, and 2011–2013). Five key land use types defined as forest, rice-wheat rotation field, urban, water, and dry land were used in this study.

The leaf area index (LAI), crop coefficient (K_c), and root depth (RD) are key dynamic vegetation properties that are directly related to precipitation canopy interception, vegetation transpiration, and total ET in forest and agricultural lands [18]. For example, forest areas had a constant RD value of 2000 mm, where the LAI values changed from 0.8 (in January) to 6 (in July) and then returned to 0.8 (in December). Changing trends of forest K_c were similar with the seasonal LAI, ranging from 0.7 to 1.1. During the full leaf period, LAI of rice and wheat had a value of 5 and 4.8, respectively. The mean K_c was set as 0.5 for rice and 0.48 for wheat at the initial stage. It was increased to 1.3 and 1.2 at the midseason stage, and was slightly decreased to 0.90 and 0.82 at the late season stage, respectively. The temporal changes of the K_c , RD, and LAI for the vegetation areas were determined by data from the literature [55–58]. In addition, irrigation management in rice paddy was taken into account. Irrigation water depths recommended by Wang et al. [59] were used to represent different growth stages of paddy rice crop (Table 2).

Table 2. Water depth meeting irrigation demand in rice-wheat rotation fields during the crop growing season [59].

Growing Stage	Irrigation Depth ($\text{mm} \cdot \text{day}^{-1}$)
Sowing	10
Tillering	20
Reviving	30
Jointing stage	30
Filling stage	40
Milky stage	30
Ripe	10

2.3.3. Meteorological Data

Daily reference evapotranspiration (ET_0) rates were calculated by daily humidity, daily radiation, daily vapor pressure, daily air temperature, daily sunlight duration, and daily wind speed at a 2 m height using the standard FAO 56 Penman–Monteith method [16]. These meteorological data for a 24-year period (1990–2013), from weather stations located within the QRB, were obtained from the China Meteorological Data Sharing Service System (<http://data.cma.cn/>). To improve model accuracy, 23 virtual stations were selected and assigned time series of precipitation and reference evapotranspiration for 1990–2013 using the ANUSPLIN meteorological interpolation method [60]; this was done because there were only a few meteorological stations in the study area.

2.3.4. Soil Data

Soil data were from the Harmonized World Soil Database (HWSD) established by the Food and Agriculture Organization of The United Nations (FAO) (<http://www.fao.org/nr/land/soils/harmonized-world-soil-database/en/>). Fifteen different types of soil were identified in the study basin (see Appendices A and B). Depth of soil layers used for unsaturated flow simulation was obtained from HWSD's database. Impervious surface parameters were set using reducing saturated hydraulic conductivity (K_s) of the upper layer. Due to lack of spatially distributed data of geological layer, single-valued hydrogeological parameters for the saturated zone were adopted within this basin.

2.3.5. Initial Conditions

Initial values, such as soil water content in the unsaturated zone and groundwater elevation in the saturated zone, play an important role in model performances [61]. The hot-start function provided by MIKE SHE was used to generate the initial conditions. This utility makes continuing simulation of different period possible.

Calculating water dynamic in saturated zone requires initial groundwater level value, i.e., "Initial Potential Head". In MIKE SHE model, the "Initial Potential Head" is the starting head for transient simulations and the initial guess for steady-state simulations [33]. In this study, this value was repeatedly adjusted until the model stabilized and produced convincing results.

2.3.6. Model Calibration and Validation

Two types of hydrological fluxes were used for model calibration and validation including monthly observed discharge data from the Wudingmen gauging station at an outlet of the Qinhuai River and daily observed ET rates data from eddy covariance technique in the rice field located at Lishui Experimental Station (Figure 1). Eddy covariance (EC) measurements of latent (LE) and sensible (H) heat were collected at 30 min intervals. It is inevitable that missing or rejected data occurred when long-term data were recorded. Data gaps less than 3 h were generally filled using linear interpolation, and gaps greater than 24 h were filled using multiple polynomial regressions [12]. We processed eddy-covariance data in the free and open-source EC software EddyPro (www.licor.com/eddypro). Energy balance closure was evaluated from 21 June 2018 to 31 July 2018. In this study, ordinary least squares (OLSs) were used to derive linear regression coefficients between the half-hourly estimates of the dependent flux variables against the independently derived available energy [62].

Hydraulic parameters were set using actual stream data in the MIKE SHE model. Calibration relies on human judgements and does not require large amounts of hydrological and meteorological data. Thirteen parameters (Table 3) were selected for model calibration according to previous studies [32,43,63].

Table 3. Key parameters controlling evapotranspiration, overland flow, drainage flow, and base flow were subject to calibration.

Water Movement	Parameter	Initial Value	Final Value	Unit
Evapotranspiration (ET)	C ₁	0.30	Forest	0.30
			Agricultural land	0.31
	C ₂	0.20	Forest	0.20
			Agricultural land	0.15
	C ₃	20	-	mm/day
C _{int}	0.05	-	mm	
Overland flow (OL)	Surface flow Manning coefficient (m)	25	Forest	5
			Urban	50
			Water	8.3
			Agricultural land	12.5
	Detention storage	10	0	mm
	Initial water depth	0	-	mm
Rivers and lakes (OC)	Channel flow Manning coefficient (m)	30	44	m ³ /s
	Leakage coefficient	1 × 10 ⁻⁷	8 × 10 ⁻⁸	/sec
Saturated flow (SZ)	Horizontal hydraulic conductivity	1 × 10 ⁻⁷	5 × 10 ⁻⁶	m/s
	Vertical hydraulic conductivity	1 × 10 ⁻⁷	1 × 10 ⁻⁶	m/s
	Storage coefficient	0.0001	5 × 10 ⁻⁵	1/m
	Time constant	1 × 10 ⁻⁶	1 × 10 ⁻⁷	/sec

This model was calibrated for four years (1991–1994) and validated for five years (1995–1999) with a one-year warm up period (1990). Moreover, 31 December 1999 was chosen as the initial condition for analyses. The calibration and validation processes were based on two statistical parameters, the coefficient of determination (R^2) and the Nash–Sutcliffe model efficiency coefficient (E) [45,51]:

$$R^2 = \frac{\sum_{i=1}^n (O_i - \bar{O})(S_i - \bar{S})}{\sqrt{\sum_{i=1}^n (O_i - \bar{O})^2} \sqrt{\sum_{i=1}^n (S_i - \bar{S})^2}} \quad (12)$$

$$E = 1 - \frac{\sum_{i=1}^n (O_i - S_i)^2}{\sum_{i=1}^n (O_i - \bar{O})^2} \quad (13)$$

where O_i and \bar{O} are observed discharge and the mean observed discharge, respectively. S_i and \bar{S} are simulation discharge and the mean simulation discharge, respectively. R^2 is the degree of similarity between the simulated and the observed runoff process. E is the accuracy of both the magnitude and timing of predicted flows. During model calibration, hydraulic parameters are optimized to allow R^2 and E to approach 1.0 [45].

2.4. Mann–Kendall Test

The Mann–Kendall (MK) test [64,65], highly recommended by the World Meteorological Organization, is a rank-based nonparametric test to detect monotonic increasing or decreasing trends in hydro-meteorological time series. This method offers many advantages, including the ability to tolerate outlier data and that normally distributed time series are not required as input [66]. In this study, we applied the MK trend test to analyze the spatial distribution of temporal trend of ET and its partitions.

For a time series $X = \{x_1, x_2, \dots, x_n\}$, the rank statistic T is given by:

$$T = \sum_{i < j} p_{ij} \quad (14)$$

where

$$p_{ij} = \text{sign}(x_j - x_i) = \text{sign}(R_j - R_i) = \begin{cases} 1 & x_i < x_j \\ 0 & x_i = x_j \\ -1 & x_i > x_j \end{cases} \quad (15)$$

where x_i and x_j are observations of the time series and R_i and R_j are their ranks, respectively. The mean and variance of the T statistic in Equation (12) are given by:

$$E(T) = 0 \quad (16)$$

$$\text{var}(T) = \frac{n(n-1)(2n+5)}{18} \quad (17)$$

$$\text{var}^*(T) = \frac{n(n-1)(2n+5)}{18} - \sum_{j=1}^m \frac{k_j(k_j-1)(2k_j+5)}{18} \quad (18)$$

$$Z = \begin{cases} \frac{T-1}{\sqrt{\text{var}(T)}} & T > 0 \\ 0 & T = 0 \\ \frac{T+1}{\sqrt{\text{var}(T)}} & T < 0 \end{cases} \quad (19)$$

where n denotes the number of observations, m denotes the number of tied ranks in groups, and k_i presents the number of data values in the i^{th} group. Z is a standardized variable. If the Z value is positive, the data exhibit an upward trend; if the Z value is negative, the data exhibit a downward trend.

In this study, the significance of trends was judged on a confidence level of $\alpha = 0.05$, where $Z_{\frac{\alpha}{2}} = 1.96$ [66]. Three types of ET and partitions trends at each pixel within this basin were determined based on their Z values with “ ≥ 1.96 ”, “ $-1.96-1.96$ ”, and “ ≤ -1.96 ” corresponding to “Increase”, “Stable”, and “Decrease”, respectively.

3. Results

3.1. Model Performance Evaluation

Monthly observed discharge data (1990–1999) from the Wudingmen gauging station were used for model calibration and validation (Figure 3). The R^2 for the regression model describing relation between simulation and observation was 0.77 for the entire study period (Figure 3a). The R^2 and E were 0.89 and 0.79, respectively, for the calibration period. In the validation period, E (0.64) was lower but R^2 was still up to 0.74. Thus, the model performance was within the acceptable range for simulating the hydrological processes in the QRB. We also simulated groundwater dynamic and found R^2 between modeled monthly groundwater level and measurements for Aiyuan well station in 2006 is 0.55 ($p = 0.01$).

The modeled ET was compared against ET measured from the flux towers (Figure 4a). Overall, the model overestimated ET, but was able to capture the seasonal patterns (Figure 4b) with an optimal R^2 of 0.72 and a slope close to 1.0 (Figure 4a). Simulated actually daily ET was close to reference evapotranspiration (ET_o) most of the time for paddy rice field (Figure 4b). ET was higher than ET_o in the fall of 2016 and 2017.

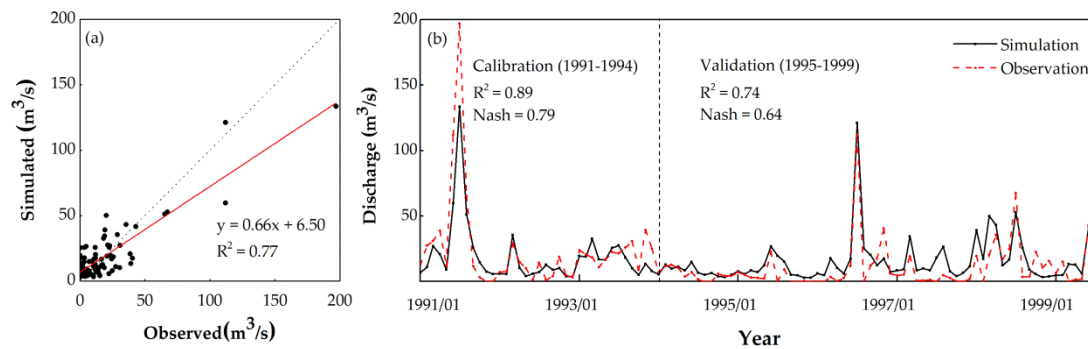


Figure 3. Monthly discharge simulated by the MIKE SHE model versus observed discharge at Wudingmen gauging station: (a) scatter plot for the period from 1991 to 1999; and (b) simulated (continuous line) and observed (dotted line) monthly hydrographs for the calibration (1991–1994) and validation (1995–1999).

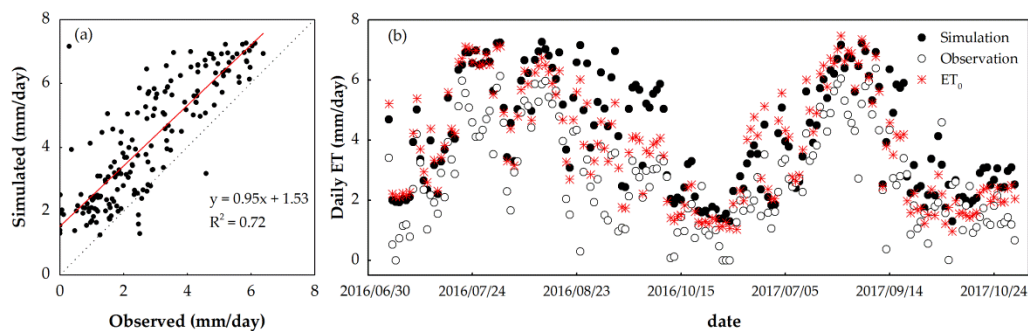


Figure 4. Comparisons between model simulated with observed daily evapotranspiration (ET) in Lishui paddy rice fields during rice growing season (from 30 June 2016 to 2 November 2016 and from 24 June 2017 to 30 October 2017): (a) scatter plot; and (b) time series comparisons of the daily simulated paddy ET derived from the MIKE SHE model, ground observed paddy ET, and average basin reference ET (ET_0).

3.2. ET and Its Components under Different Land Use Types

Annual ET_0 presented a significant upward trend at the rate of 11.4 mm/year ($p < 0.01$) (Figure 5). Nevertheless, annual watershed level ET exhibited an opposite trend. T , E_i , and E_s exhibited a downward trend, which were partially counteracted by water surface evaporation (E_p) increasing. The total decrease rates for T , E_i , and E_s were about 2.5 times as much as the total increase of E_p .

Watershed scale T was about 53% of ET , the highest proportion among all ET partitions. The ratio of T to ET showed a negative trend, decreasing from 60% in 2000 to 53% in 2013 (Figure 6). The secondary contributor was E_s (140 mm/year), showing a slight decrease. In contrast, E_p significantly increased from 66 mm/year in 2000 to 153 mm/year in 2013 ($p < 0.05$). In addition, the range of long-term variation in E_s and E_i was very similar, and was less than the range of T and E_p .

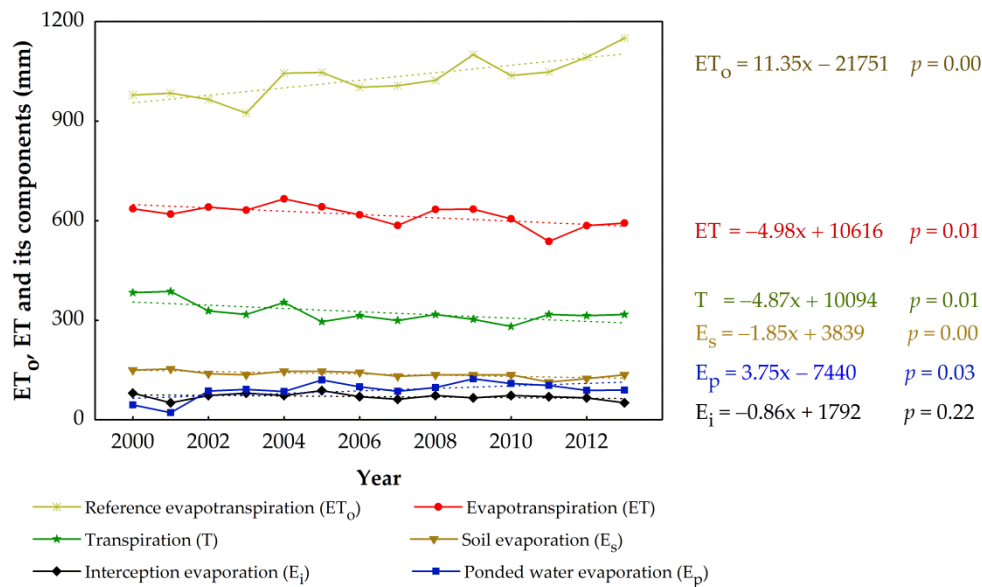


Figure 5. Trend of annual watershed-level reference evapotranspiration (ET_o), evapotranspiration (ET), and its partitioning in the Qinhuai River Basin from 2000 to 2013.

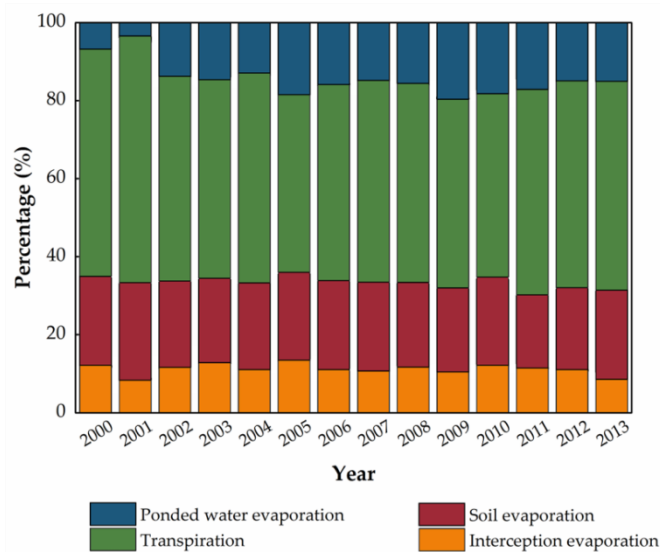


Figure 6. Simulated mean annual proportion of evapotranspiration partitioning in the Qinhuai River Basin from 2000 to 2013.

Land-cover types affect the hydrological cycle including ET partitions. On average, E_p accounted for 20% of rice-wheat rotation field ET (ET_{r-w}) during 2000–2013, becoming the second dominant source of water loss exceeding the contribution of E_s to ET (Figure 7). On the contrary, E_s of non-irrigated forest and dry land was much greater than E_p , making up 12.9% and 28.9% of ET, respectively. T was the overwhelming contributor to forest, rice-wheat rotation field, and dry land ET, accounting for 71.5%, 53.4%, and 42.8%, respectively. E_i remained low compared to other partitions but cannot be discounted. Mean E_i of forest, rice-wheat rotation field, and dry land was about 11.9%, 10.5%, and 15.2% of ET, respectively.

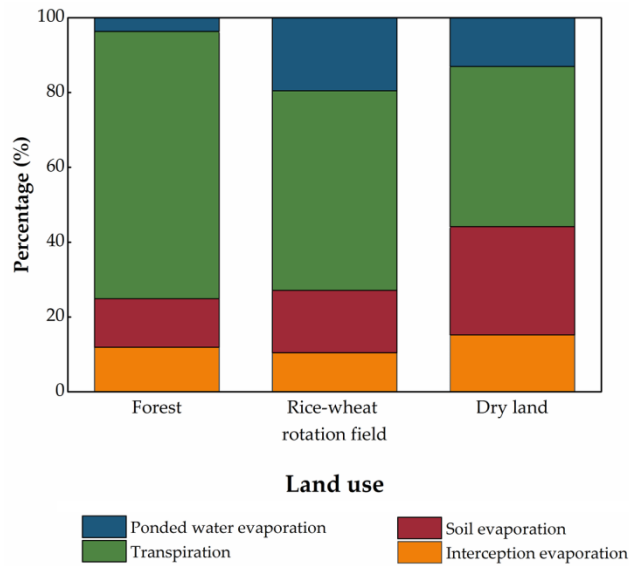


Figure 7. Average proportion of evapotranspiration partitioning with three types of vegetation (2000–2013).

For urban area, we were not able to discern the particular plant types. Therefore, we simplified the model and did not take into account vegetation within urban area. The whole urban area was assumed impervious surface with zero ET.

The averaged annual forest ET (ET_f) was 950 mm over 14 years. Annual dry land ET (ET_d) was about half of rice-wheat ET (ET_{r-w}) (Figure 8). The T rate (656 mm/year) of forest was the highest, followed by that of rice-wheat rotation field and dry land. Mean annual rice-wheat rotation field E_p (per unit area) was highest among different land use types (about 167 mm) due to irrigation. These results imply that the conversion of forests or rice-wheat rotation field to urban had more impacts on the change in ET and its partition than the conversion of other land-cover change scenarios. In addition, annual ET and T of forest and rice-wheat rotation field were higher than the catchment scale, and E_p of rice-wheat rotation field was twice that of the whole catchment, showing expansion in urban area had unfavorable effects on catchment ET over this basin.

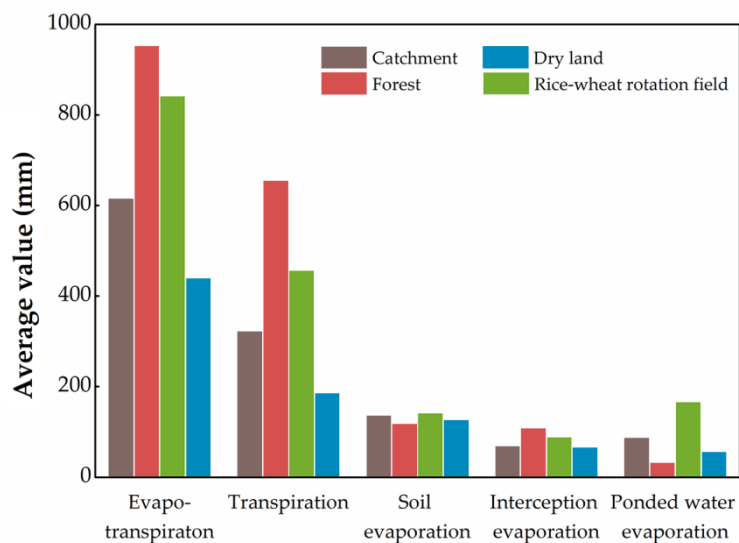


Figure 8. A comparison of mean annual evapotranspiration and its components at land use type and whole catchment scales (2000–2013) for the Qinhuai River Basin.

The total catchment ET in volume significantly declined from $1654 \times 10^6 \text{ m}^3$ in 2000 to $1542 \times 10^6 \text{ m}^3$ in 2013 (Figure 9b). The total ET_f and ET_d increased, similar to the grid scale (Figure 9). However, the total ET_{r-w} exhibited a significant decrease ($p < 0.01$), opposite to the pattern at field scale expressed in per unit area, which was associated with the loss of rice-wheat rotation fields. Although forest generated more ET per unit area than rice-wheat rotation field (Figure 8), the decline in the total ET_{r-w} was one of the primary factors responsible for the significant decline trend of ET because of large water volume per unit area (840 mm/year) and large area of rice-wheat rotation field.

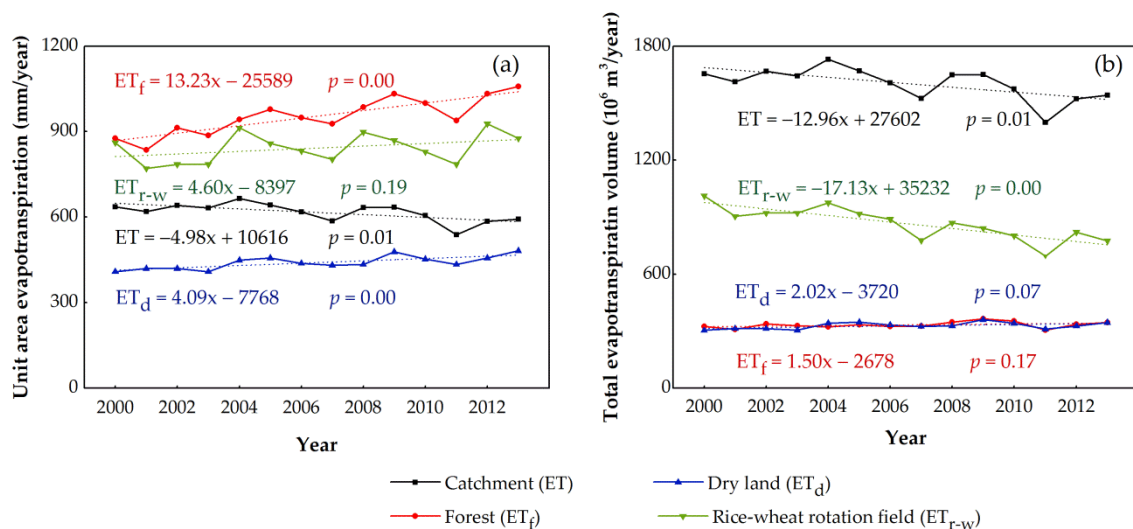


Figure 9. A comparison of the temporal trends from 2000 to 2013 for the Qinhuai River Basin: (a) mean annual evapotranspiration at the pixel scale; and (b) total evapotranspiration volume by land use types.

3.3. Spatial Variability of ET Components and Annual Water Balance

About 27% of the QRB that was dominated by forest and agricultural land areas had a significant positive ET trend (Figure 10), while ET of the area transformed into urban landscape exhibited a significant downward trend. As for T, a clear increase trend occurred in the southeast part of the QRB dominated by forests and croplands, while an opposite trend was seen in the northwest part of the watershed covered by an urban area where E_s also exhibited a significant reduction.

It was estimated that 60.4%, 40.2%, and 10.2% of forest, dry land, and rice-wheat rotation field had a significant increasing trend in ET, respectively (Figure 10). For T, 38.8%, 24.9%, and 1.4% of forest, dry land, and rice-wheat rotation field exhibited a significant upward trend, while 15.6%, 18.1%, and 31% of forest, dry land, and rice-wheat rotation field exhibited a significant downward trend. The watershed showed a significant increasing trend in E_s in 50.7%, 34.3%, and 5.6% of forest, dry land, and rice-wheat rotation field, respectively. E_i of all land cover types had about 10–12% the areas classified as "Decrease". About 11% of the rice-wheat rotation field had a growing trend in E_p .

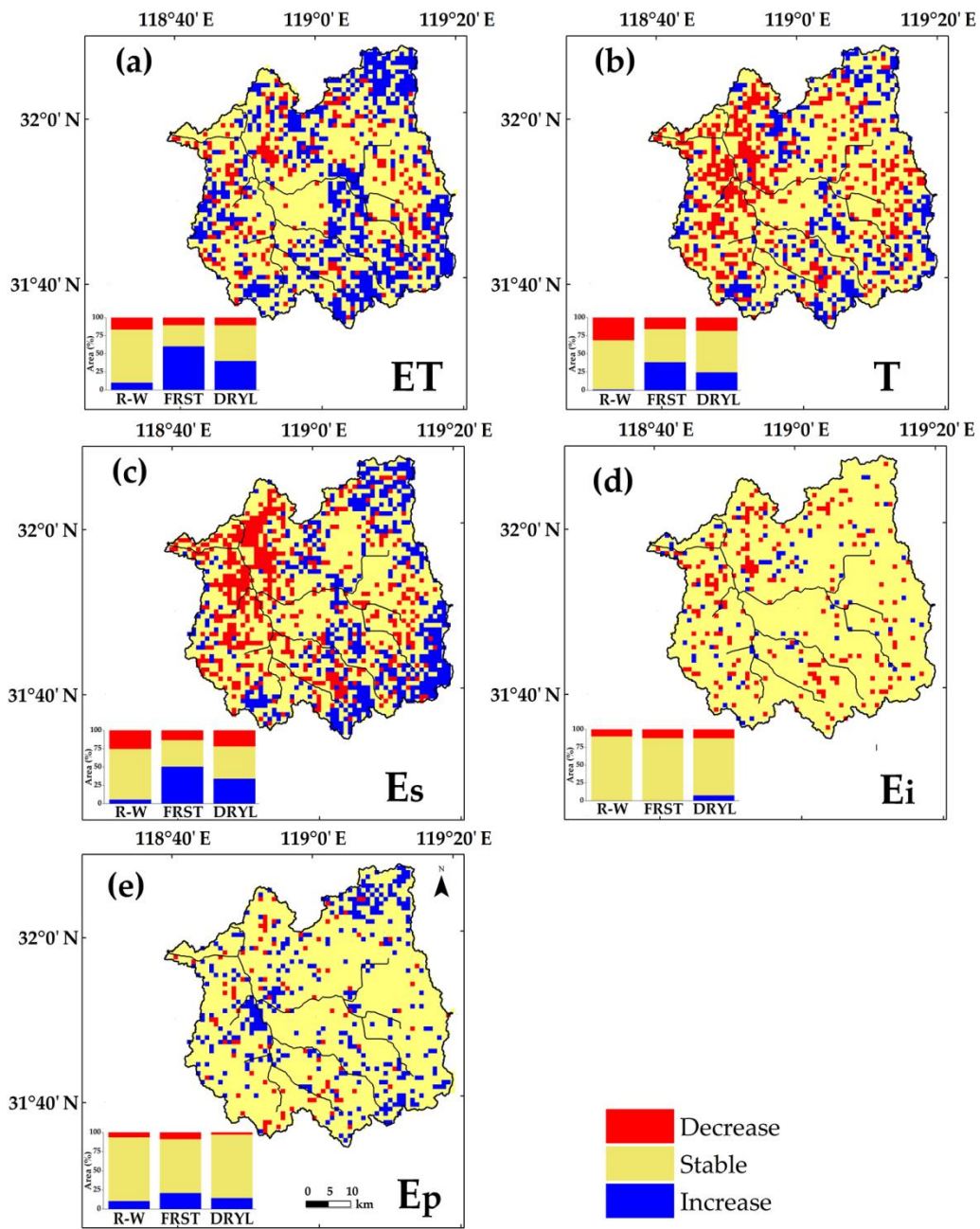


Figure 10. Spatial trends from 2000 to 2013 in: evapotranspiration ET (a); transpiration T (b); soil evaporation E_s (c); interception evaporation E_i (d); and ponded water evaporation E_p (e). Three distinct areas in ET and components trends are identified as “Increase”, “Stable”, and “Decrease”. The area percentage bars of rice-wheat field (R-W), forest (FRST), and dry land (DRYL) are based on land use in 2000.

Although not significant statistically, annual simulated runoff (Q_s) was predicted to increase from 336 mm in 2000 to 412 mm in 2013 at the rate of 7 mm/year (Figure 11). The measured annual runoff (Q_m) ($p = 0.05$) and simulated annual runoff (Q_s) ($p = 0.57$) both exhibited a positive trend while annual ET decreased significantly. Large annual values of Q_s were found in 2003 and 2009 with the values of 813 and 850 mm, respectively, corresponding to two wet years.

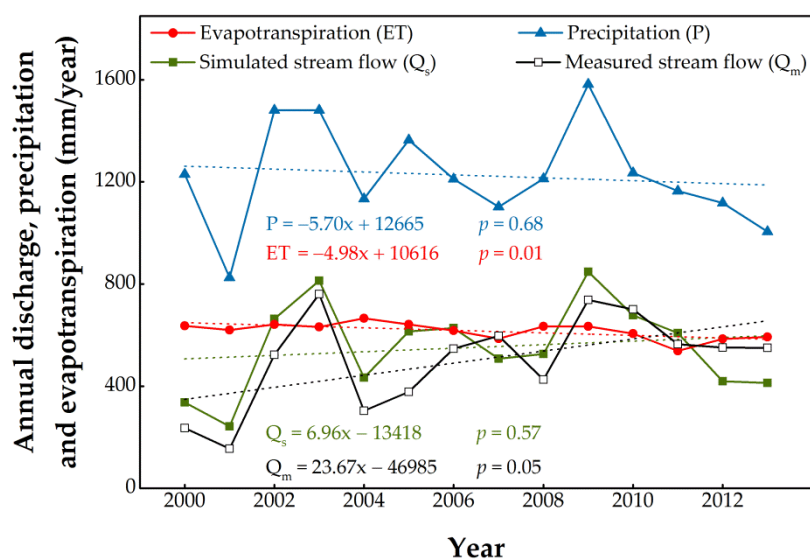


Figure 11. Changes of annual measured stream flow (Q_m), simulated stream flow (Q_s), evapotranspiration (ET), and precipitation (P) for the Qinhuai River basin from 2000 to 2013.

4. Discussion

4.1. Effects of Land Use and Land Cover Changes on all ET Components

ET and its partitions in watershed with mixed land use are complex because heterogeneous landscape is a patchwork of vegetation (i.e., trees, shrubs, and grass) and buildings [67]. In dry regions, urban ET may be much higher than the surrounding natural landscape due to external water sources such as groundwater or inter-basin water transfer [68]. However, many studies supported our result that ET rates in urban area were small due to the loss of green areas in humid regions [69–71]. Nanjing, Lishui, and Jurong cities from our study basin are highly urbanized [23,43], and the vegetation cover is especially lacking [72]. Litvak et al. [67] found that ET was minor for bare soil and concrete land surface.

The consistent trends between ET with each land use type and ET_o demonstrated that meteorological factors were controlling factors for ET at the pixel scale. However, we showed that watershed-level ET had a significant decreasing trend in the QRB, coincident with previous studies [2,42]. This was in contrast to the global warming trend and ET was expected to increase under increasing air temperature in the study region [73–75]. Declines in ET have also been reported in the literature around the world, such as eastern China [76], Haihe River Basin [77], Liaohe River Delta [78], and the southern hemisphere in Africa [79]. In our case, 16.5% of rice-wheat rotation fields with high ET were converted into urban area characterized by low vegetation coverage with low ET from 2000 to 2013. Thus, the watershed hydrological cycle has been altered [2,6,34,69]. An early study by Hao et al. [2] confirmed that the remarkable impacts land use and land cover change have overwhelmed the effects of climate in the QRB. Previous studies also suggested that converting water stress-free rice-wheat rotation fields to relatively “dry” urban area has a much larger impact on regional water balances than converting dry lands or forests to urban [2,7]. The present study extended previous findings by offering new insights of ET partitions temporally and spatially in the QRB.

Rice-wheat rotation fields require large amounts of water to sustain productivity and are rarely under water stress due to abundant irrigation inputs during the rice growing season [80,81]. The rice-wheat rotation fields dominated the QRB and were responsible for a large portion of basin water loss by transpiration and soil evaporation. However, it suffered the most significant loss of acreage when compared to other land uses (Figure 2a). Thus, owing to converting rice-wheat rotation fields to urban areas, increasing paved areas with low T and E_s caused the pronounced decrease in T and E_s , which inevitably affected the catchment ET (Figure 5).

Urbanization influences ecosystems through altering water cycles [1,23,82]. The response of ET and its partitions in the QRB is one of the strongest pieces of evidence for this. Our findings were similar to result by Liu et al. [4] that the impacts of land use and land cover changes on the water cycle were represented by E_i , E_s , and T . Olchev et al. [83] found that the conversion of natural forests to urban and residential uses reduced ET as a result of declines in T and E_i . Litvak et al. [67] showed that annual ET from the whole Los Angeles city was three times smaller than ET from vegetated landscapes, and they attributed it to the reduction in evapotranspiration from trees and well-irrigated turfgrass due to urbanization.

4.2. Effects of Urbanization and ET on Mean Annual Runoff

The annual water balance for the QRB over 14 years has been altered as a result of rapid urbanization (Figure 11). A 175% expansion of urban area throughout the QRB led to a 23% increase in annual runoff depths. This finding is consistent with studies that reported urbanization promoted quick runoff [6,46,84]. Im et al. [85] studied future land use scenarios impacted on the hydrology of the Polecat Creek watershed, US, with a modeling approach and found that streamflow volume increased 15.8% when an increases in impervious areas of up to 10.1%. Dietz and Clausen [84] revealed that stormwater runoff increased by more than two orders of magnitude in the development zone from 1997 to 2003. However, the impact of urbanization on annual runoff is extremely variable [2]. Franczyk and Chang [86] predicted that mean annual runoff had hardly changed in the Rock Creek basin, Portland, with an increase of only 2.3–2.5% when the impervious ratio increased by 8–15%, respectively. One possible explanation for this phenomenon is that the baseflow is reduced while the direct runoff increases due to urban area expansion, and consequently the total runoff volume does not change considerably [6].

The elevated watershed runoff volume due to urban expansion was not only related to an increase in impervious surface but also to a decrease in ET rate. For example, Boggs and Sun [7] compared seasonal flow and ET patterns between an urbanized watershed and a fully forested watershed in the southeastern United States and found that the hydrology of the two watersheds was similar in the dormant season with low tree transpiration but highly different in the peak growing season. In addition, Im et al. [46] found that reducing groundwater recharge and ET rate caused a significant increase in surface runoff with a rapid urban development. Thus, for an urbanizing watershed, maintaining ET capacity of vegetation, the “biological drainage”, is a vital prerequisite for reducing stormflow [7,46].

4.3. Implications of ET Reduction to Regional Ecosystem Productivity and Environment

T in areas covered by vegetation in the QRB was a major contributor to ET (Figure 7), and thus change in T was likely to affect total water loss from the study watershed. Our study showed that forests had the highest T rate (656 mm/year), followed by rice-wheat rotation field (460 mm/year) and dry land (190 mm/year) (Figure 8). T was sensitive to changes in plant types and temporal vegetation dynamics [21]. Urbanization may result in the expansion of impervious surfaces with no vegetation, resulting in reduction of T and ET. It is understandable that, when rice-wheat rotation fields were removed, their water retention and ET functions (i.e., water pumps) were lost, leading to increase in runoff

In addition, ET is a major factor affecting land surface energy balances and thus micro-climate [23]. Our results complement an earlier research in the same study area. Hao et al. [69] concluded that reduction of ET caused by the loss of vegetation cover (i.e., natural wetlands and rice-wheat rotation fields) was a vital factor contributing to the urban dry island (UDI) effects (i.e., reduction of air humidity due to decrease in ET) and the well-known urban heat island (UHI) effects. Our data show that annual T decreased sharply in the context of the massive conversion of rice-wheat rotation field to urban land use. Thus, our new analysis suggested that significantly reduced T could be the dominant cause that contributed to the changes of regional environment, including the UDI and UHI effects in the QRB.

Changes in T may also affect local precipitation patterns. Lee et al. [87] compared results with and without transpiration from the National Center for Atmospheric Research (NCAR) atmospheric general circulation model and pointed out that the absence of transpiration led to decreased mean precipitation and increased the variability of precipitation. An increasingly regional precipitation variability due to decreasing T poses a risk to human health and has implications to agriculture [87,88]. T acts as an important source of moisture and plays a vital role in moisture recycling, which is expected to be of great significance for water resources, agriculture, and ecosystems [89–91]. Thus, in the QRB, significant reduction in T could attenuate the local moisture recycling, and thus enhance drought vulnerability [89] and reduce crop yield [92].

4.4. Uncertainty

The strength of the MIKE SHE model is its capacity to model the spatial variability of hydrological processes [32,45,93]. However, at the same time, the power of representation of spatial variability of hydrological characteristics is its weakness [47]. For example, there are parameter uncertainties about the soils and geology, as well as different vegetation on a fragmented landscape in QRB. Because detailed geological layer information in QRB is not available, homogenous hydrogeological parameters of one geological layer were implemented within the whole catchment, which may impact the groundwater dynamics and in turn impact ET processes [45,50]. However, Sahoo et al. [94] stated that the well-calibrated MIKE SHE model having the single-valued hydrogeological parameters can produce convincing outcomes. Thus, to avoid over-parameterization and weaken the physical meanings of the parameters, we simplified the parameterization of the groundwater system. Future studies are needed to evaluate how this treatment affects spatial distributions of groundwater table dynamics and ET rates. Such model validations are essential to take the full advantages of the capacity of MIKE SHE in simulating surface water–groundwater interactions and the effects of urbanization on ET and runoff at multiple scales.

Another major source of uncertainty about ET modeling results is a lack of validation data, including ET measurements for different land cover types. More measurements on actual ET partitions are necessary to further improve the MIKE SHE model. Furthermore, information of observed ET rates at the flux site is only available in recent years. We were unable to validate paddy ET in previous years that might have different precipitation patterns. This deficiency may introduce uncertainty in quantifying actual ET patterns in paddy rice system. Moreover, because discerning particular plant types in urban area at the 1000 m spatial resolution is challenging, we excluded vegetation in urban land areas. This treatment may have caused errors to some extent, which could lead to the model uncertainty in estimating urban ET. Future study should obtain spatially and temporally distributed land cover data at a finer spatial resolution by coupling remotely sensed satellite products or field investigations. Water and energy balances in urban areas are not well understood, and future studies should be conducted in urban areas with a mixed land use, especially in humid regions.

5. Conclusions

This study used a distributed hydrologic model, MIKE SHE, to spatially explicitly estimate ET partitions in the Qinhuai River Basin (QRB) from 2000 to 2013. Over the QRB, conversion of rice-wheat rotation field to urban had more impacts on ET and its partition than other land covers. Vegetation transpiration (T), canopy interception (E_i), and soil evaporation (E_s) showed a downward trend, while ponded water evaporation (E_p) increased. T reduced most sharply due to urbanization, resulting in a significant decline of watershed-level ET. Urbanization elevated runoff by decreasing the ET rates.

Our research combines technology of advanced hydrological modeling and remote sensing products. This approach allows better estimates of changes of watershed ET and its partitions due to changes in climate and urbanization. However, parameterizing a complex hydrological model at the basin scale is still challenging and validating the spatial distribution of ET and runoff is still lacking.

Our findings imply that a significant decrease in T due to urbanization is likely to cause large impacts on water yield, regional ecosystem productivity, local moisture cycling, droughts, UDI and UHI in the study basin. Urban planning and watershed restoration measures in the humid region should consider all the benefits of vegetation to reduce risk to ecosystems and humans.

Author Contributions: Conceptualization, L.H., G.S. and Q.Z.; methodology, Q.Z.; software, Q.Z. and L.S.; validation, L.H., G.S. and Q.Z.; formal analysis, L.H., G.S. and Q.Z.; investigation, Q.Z. and X.H.; resources, L.H.; data curation, L.H., L.S., X.H. and Q.Z.; writing—original draft preparation, L.H. and Q.Z.; writing—review and editing, L.H., G.S. and Q.Z.; supervision, L.H. and G.S.; project administration, L.H.; funding acquisition, L.H. All authors have read and agreed to the published version of the manuscript.

Funding: This research was funded by the National Natural Science Foundation of China, grant number 41877151, 41571026, and 41977409.

Acknowledgments: We acknowledge China Meteorological Data Service Center (<http://data.cma.cn/en>) for providing daily weather observation data; and National Earth System Science Data Sharing Infrastructure, National Science & Technology Infrastructure of China (www.geodata.cn) for sharing land use and land cover data and the digital elevation model (DEM) of the Qinhui river basin. Partial support was also received from the Southern Research Station, United States Department of Agriculture Forest Service.

Conflicts of Interest: The authors declare no conflict of interest.

Appendix A

Table A1. The key soil physical parameters of upper soil layer.

Soil Profile ID	Field Capacity	Wilting Point	Saturated Hydraulic Conductivity (m/s)
11368	0.41	0.28	1.8×10^{-6}
11373	0.36	0.17	1.3×10^{-5}
11376	0.28	0.14	1.4×10^{-6}
11389	0.28	0.14	1.2×10^{-6}
11489	0.42	0.29	2.1×10^{-6}
11613	0.30	0.17	1.3×10^{-6}
11617	0.39	0.26	1.6×10^{-6}
11649	0.30	0.06	6.0×10^{-5}
11656	0.30	0.17	1.3×10^{-6}
11663	0.40	0.24	2.5×10^{-6}
11823	0.30	0.17	1.3×10^{-6}
11857	0.12	0.06	1.0×10^{-5}
11859	0.27	0.14	9.3×10^{-7}
11875	0.39	0.26	1.5×10^{-6}
11876	0.27	0.13	1.2×10^{-6}

Appendix B

Table A2. The key soil physical parameters of subsoil layer.

Soil Profile ID	Field Capacity	Wilting Point	Saturated Hydraulic Conductivity (m/s)
11368	0.43	0.32	2.0×10^{-6}
11373	0.31	0.16	1.8×10^{-6}
11376	0.25	0.14	1.0×10^{-6}
11389	0.26	0.14	1.1×10^{-6}
11489	0.41	0.28	1.7×10^{-6}

Table A2. Cont.

Soil Profile ID	Field Capacity	Wilting Point	Saturated Hydraulic Conductivity (m/s)
11613	0.28	0.14	9.9×10^{-7}
11617	0.39	0.24	1.5×10^{-6}
11649	0.09	0.05	3.8×10^{-5}
11656	0.28	0.14	9.9×10^{-7}
11663	0.22	0.07	4.6×10^{-7}
11823	0.35	0.22	8.1×10^{-7}
11857	0.17	0.10	3.6×10^{-6}
11859	0.31	0.18	6.5×10^{-7}
11875	0.43	0.31	1.8×10^{-6}
11876	0.35	0.22	8.1×10^{-7}

References

- Razali, A.; Ismail, S.N.S.; Awang, S.; Praveena, S.M.; Abidin, E.Z. Land use change in highland area and its impact on river water quality: A review of case studies in Malaysia. *Ecol. Process.* **2018**, *1*, 19. [\[CrossRef\]](#)
- Hao, L.; Sun, G.; Liu, Y.; Wan, J.; Qin, M.; Qian, H.; Liu, C.; Zheng, J.; John, R.; Fan, P. Urbanization dramatically altered the water balances of a paddy field dominated basin in Southern China. *Hydrol. Earth Syst. Sci.* **2015**, *7*, 3319–3331. [\[CrossRef\]](#)
- Oudin, L.; Salavati, B.; Furusho-Percot, C.; Ribstein, P.; Saadi, M. Hydrological impacts of urbanization at the catchment scale. *J. Hydrol.* **2018**, *559*, 774–786. [\[CrossRef\]](#)
- Liu, X.; Ren, L.; Yuan, F.; Singh, V.P.; Fang, X.; Yu, Z.; Zhang, W. Quantifying the effect of land use and land cover changes on green water and blue water in northern part of China. *Hydrol. Earth Syst. Sci.* **2009**, *6*, 735–747. [\[CrossRef\]](#)
- Choi, W.; Deal, B.M. Assessing hydrological impact of potential land use change through hydrological and land use change modeling for the Kishwaukee River basin (USA). *J. Environ. Manag.* **2008**, *4*, 1119–1130. [\[CrossRef\]](#)
- Du, J.; Qian, L.; Rui, H.; Zuo, T.; Zheng, D.; Xu, Y.; Xu, C.Y. Assessing the effects of urbanization on annual runoff and flood events using an integrated hydrological modeling system for Qinhuai River basin, China. *J. Hydrol.* **2012**, *5*, 127–139. [\[CrossRef\]](#)
- Boggs, J.L.; Sun, G. Urbanization alters watershed hydrology in the Piedmont of North Carolina. *Ecohydrology* **2011**, *2*, 256–264. [\[CrossRef\]](#)
- Liu, X.; Pei, F.; Wen, Y.; Li, X.; Wang, S.; Wu, C.; Cai, Y.; Wu, J.; Chen, J.; Feng, K. Global urban expansion offsets climate-driven increases in terrestrial net primary productivity. *Nat. Commun.* **2019**, *1*, 1–8. [\[CrossRef\]](#)
- Li, C.; Sun, G.; Cohen, E.; Zhang, Y.; Xiao, J.; McNulty, S.G.; Meentemeyer, R.K. Modeling the Impacts of Urbanization on Watershed-scale Gross Primary Productivity and Tradeoffs with Water Yield across the Conterminous United States. *J. Hydrol.* **2020**, *583*, 124581. [\[CrossRef\]](#)
- Peng, F.; You, Q.; Xue, X.; Guo, J.; Wang, T. Evapotranspiration and its source components change under experimental warming in alpine meadow ecosystem on the Qinghai-Tibet plateau. *Ecol. Eng.* **2015**, *84*, 653–659. [\[CrossRef\]](#)
- Sun, G.; Lockaby, B.G. Water quantity and quality at the urban–rural interface. *Urban Rural Interfaces Link. People Nat.* **2012**, 29–48. [\[CrossRef\]](#)
- Lin, Y.; Wang, G.X.; Guo, J.Y.; Sun, X.Y. Quantifying evapotranspiration and its components in a coniferous subalpine forest in Southwest China. *Hydrol. Process.* **2012**, *20*, 3032–3040. [\[CrossRef\]](#)
- Newman, B.D.; Wilcox, B.P.; Archer, S.R.; Breshears, D.D.; Dahm, C.N.; Duffy, C.J.; McDowell, N.G.; Phillips, F.M.; Scanlon, B.R.; Vivoni, E.R. Ecohydrology of water-limited environments: A scientific vision. *Water Resour. Res.* **2006**, *42*, 6. [\[CrossRef\]](#)
- Yermiyahu, U.; Tal, A.; Ben-Gal, A.; Bar-Tal, A.; Tarchitzky, J.; Lahav, O. Rethinking desalinated water quality and agriculture. *Science* **2007**, *5852*, 920–921. [\[CrossRef\]](#)
- Raz-Yaseef, N.; Dan, Y.; Schiller, G.; Cohen, S. Dynamics of evapotranspiration partitioning in a semi-arid forest as affected by temporal rainfall patterns. *Agric. For. Meteorol.* **2012**, *2*, 77–85. [\[CrossRef\]](#)

16. Allen, R.G.; Pereira, L.S.; Raes, D.; Smith, M. *Crop Evapotranspiration—Guidelines for Computing Crop Water Requirements—FAO Irrigation and Drainage Paper 56*; FAO: Rome, Italy, 1998; Volume 9.
17. Xiao, W.; Wei, Z.; Wen, X. Evapotranspiration partitioning at the ecosystem scale using the stable isotope method—A review. *Agric. For. Meteorol.* **2018**, *263*, 346–361. [[CrossRef](#)]
18. Wang, L.; Good, S.P.; Caylor, K.K. Global synthesis of vegetation control on evapotranspiration partitioning. *Geophys. Res. Lett.* **2014**, *19*, 6753–6757. [[CrossRef](#)]
19. Wang, W.; Li, J.; Yu, Z.; Ding, Y.; Xing, W.; Lu, W. Satellite retrieval of actual evapotranspiration in the Tibetan Plateau: Components partitioning, multidecadal trends and dominated factors identifying. *J. Hydrol.* **2018**, *559*, 471–485. [[CrossRef](#)]
20. Kool, D.; Agam, N.; Lazarovitch, N.; Heitman, J.L.; Sauer, T.J.; Ben-Gal, A. A review of approaches for evapotranspiration partitioning. *Agric. For. Meteorol.* **2014**, *1*, 56–70. [[CrossRef](#)]
21. Tong, Y.; Wang, P.; Li, X.-Y.; Wang, L.; Wu, X.; Shi, F.; Bai, Y.; Li, E.; Wang, J.; Wang, Y. Seasonality of the transpiration fraction and its controls across typical ecosystems within the Heihe River Basin. *J. Geophys. Res. Atmos.* **2019**, *124*, 1277–1291. [[CrossRef](#)]
22. Schlaepfer, D.R.; Ewers, B.E.; Shuman, B.N.; Williams, D.G.; Frank, J.M.; Massman, W.J.; Lauenroth, W.K. Terrestrial water fluxes dominated by transpiration: Comment. *Ecosphere* **2016**, *5*, 1–9. [[CrossRef](#)]
23. Sun, G.; Hallema, D.; Asbjornsen, H. Ecohydrological processes and ecosystem services in the Anthropocene: A review. *Ecol. Process.* **2017**, *1*, 1–9. [[CrossRef](#)]
24. Yezpe, E.A.; Huxman, T.E.; Ignace, D.D.; English, N.B.; Weltzin, J.F.; Castellanos, A.E.; Williams, D.G. Dynamics of transpiration and evaporation following a moisture pulse in semiarid grassland: A chamber-based isotope method for partitioning flux components. *Agric. For. Meteorol.* **2005**, *3–4*, 359–376. [[CrossRef](#)]
25. Brunel, J.P.; Walker, G.R.; Dighton, J.C.; Monteny, B. Use of stable isotopes of water to determine the origin of water used by the vegetation and to partition evapotranspiration. A case study from HAPEX-Sahel. *J. Hydrol.* **1997**, *1*, 466–481. [[CrossRef](#)]
26. Lu, Q. *Spatiotemporal Variation of T/ET in Forest Ecosystems along the North South Transect of East China*; University of Chinese Academy of Sciences: Beijing, China, 2015. (In Chinese)
27. Mu, Q.; Heinsch, F.A.; Zhao, M.; Running, S.W. Development of a global evapotranspiration algorithm based on MODIS and global meteorology data. *Remote Sens. Environ.* **2007**, *4*, 519–536. [[CrossRef](#)]
28. Shuttleworth, W.J.; Wallace, J. Evaporation from sparse crops—An energy combination theory. *Q. J. R. Meteorol. Soc.* **1985**, *469*, 839–855. [[CrossRef](#)]
29. Gharsallah, O.; Facchi, A.; Gandolfi, C. Comparison of six evapotranspiration models for a surface irrigated maize agro-ecosystem in Northern Italy. *Agric. Water Manag.* **2013**, *130*, 119–130. [[CrossRef](#)]
30. Ferreira, M.I.; Silvestre, J.; Conceição, N.; Malheiro, A.C. Crop and stress coefficients in rainfed and deficit irrigation vineyards using sap flow techniques. *Irrig. Sci.* **2012**, *5*, 433–447. [[CrossRef](#)]
31. Fisher, J.B.; Tu, K.P.; Baldocchi, D.D. Global estimates of the land–atmosphere water flux based on monthly AVHRR and ISLSCP-II data, validated at 16 FLUXNET sites. *Remote Sens. Environ.* **2008**, *3*, 901–919. [[CrossRef](#)]
32. Wang, S. *Eco-Hydrological Response of Small Watershed to Land Use Change and Climate Variation*; Beijing Forestry University: Beijing, China, 2007. (In Chinese)
33. DHI. *MIKE SHE Technical Reference. Version 2005*; DHI Water and Environment: Hørsholm, Denmark, 2005.
34. Du, J.; Li, C.; Rui, H.; Qian, L.; Zheng, D.; Xu, Y.; Hu, S. The change detection of impervious surface and its impact on runoff in the Qinhuai River Basin, China. *Int. Conf. Geoinform.* **2011**, 1–5. [[CrossRef](#)]
35. He, B.; Wang, Y.; Takase, K.; Mouri, G.; Razafindrabe, B.H.N. Estimating Land Use Impacts on Regional Scale Urban Water Balance and Groundwater Recharge. *Water Resour. Manag.* **2009**, *9*, 1863–1873. [[CrossRef](#)]
36. Davis, J.A.; Froend, R. Loss and degradation of wetlands in southwestern Australia: Underlying causes, consequences and solutions. *Wetl. Ecol. Manag.* **1999**, *7*, 13–23. [[CrossRef](#)]
37. Liu, S.; Zhang, L.; Liu, Q.; Zou, J. Fe(III) fertilization mitigating net global warming potential and greenhouse gas intensity in paddy rice-wheat rotation systems in China. *Environ. Pollut.* **2012**, *164*, 73–80. [[CrossRef](#)] [[PubMed](#)]
38. Zhao, L.; Li, W.; Lin, L.; Guo, W.; Zhao, W.; Tang, X.; Gong, D.; Li, Q.; Xu, P. Field Investigation on River Hydrochemical Characteristics and Larval and Juvenile Fish in the Source Region of the Yangtze River. *Water* **2019**, *11*, 1342. [[CrossRef](#)]

39. Wang, Z.; Wang, Z.; Bai, Z.; Lu, C.; Ren, C. Impact of land use/land cover changes on ecosystem services in the Nenjiang River Basin, Northeast China. *Ecol. Process.* **2015**, *4*, 11. [[CrossRef](#)]
40. Sun, G.; Caldwell, P. Impacts of urbanization on stream water quantity and quality in the United States. *Water Resour. Impact* **2015**, *1*, 17–20.
41. Li, C. *The Extract Impervious Surface and Its Effect on Hydrological on the Qinhuai River Basin*; Nanjing University: Nanjing, China, 2011. (In Chinese)
42. Qin, M.; Hao, L.; Sun, L.; Liu, Y.; Sun, G. Climatic Controls on Watershed Reference Evapotranspiration Varied during 1961–2012 in Southern China. *J. Am. Water Resour. Assoc.* **2019**, *1*, 189–208. [[CrossRef](#)]
43. Sun, L. *Simulating the Effects of Land Use/Cover Change on the Key Ecological Hydrological Processes in a Paddyfield-Dominated Basin*; Nanjing University of Information Science and Technology: Nanjing, China, 2017. (In Chinese)
44. Wen, Z.; Wang, B.; Lu, C.; Yan, L.; Hua, H. Development and utilization division of groundwater resources in Nanjing city. *J. Jilin Univ.* **2009**, *1*, 109–115.
45. Lu, X. *Hydrology Response in Different Scales Using Surface Water and Groundwater Coupling Model: Case Studies in Skjern Catchment of Denmark and the North China Plain*; Chian University of Geosciences: Beijing, China, 2009. (In Chinese)
46. Im, S.; Kim, H.; Kim, C.; Jang, C. Assessing the impacts of land use changes on watershed hydrology using MIKE SHE. *Environ. Geol.* **2009**, *1*, 231–239. [[CrossRef](#)]
47. Feyen, L.; Vázquez, R.; Christiaens, K.; Sels, O.; Feyen, J. Application of a distributed physically-based hydrological model to a medium size catchment. *Hydrol. Earth Syst. Sci.* **2000**, *1*, 47–63. [[CrossRef](#)]
48. Abbott, M.; Bathurst, J.; Cunge, J.; O’connell, P.; Rasmussen, J. An introduction to the European Hydrological System—Systeme Hydrologique Europeen “SHE”, 2: Structure of a physically-based, distributed modelling system. *J. Hydrol.* **1986**, *87*, 61–77. [[CrossRef](#)]
49. Cochand, M.; Molson, J.; Lemieux, J.M. Groundwater hydrogeochemistry in permafrost regions. *Permafr. Periglac. Process.* **2019**, *2*, 90–103. [[CrossRef](#)]
50. Goderniaux, P.; Brouyère, S.; Fowler, H.J.; Blenkinsop, S.; Therrien, R.; Orban, P.; Dassargues, A. Large scale surface–subsurface hydrological model to assess climate change impacts on groundwater reserves. *J. Hydrol.* **2009**, *1–2*, 122–138. [[CrossRef](#)]
51. Dai, Z.; Li, C.; Trettin, C.; Sun, G.; Amatya, D.; Li, H. Bi-criteria evaluation of the MIKE SHE model for a forested watershed on the South Carolina coastal plain. *Hydrol. Earth Syst. Sci.* **2010**, *6*, 1033–1046. [[CrossRef](#)]
52. Richards, K.L.; Cannon, S.R.; Miller, J.F.; Crawford, M.H. Calculation of aortic valve area by Doppler echocardiography: A direct application of the continuity equation. *Circulation* **1986**, *5*, 964–969. [[CrossRef](#)] [[PubMed](#)]
53. Kristensen, K.; Jensen, S. A model for estimating actual evapotranspiration from potential evapotranspiration. *Hydrol. Res.* **1975**, *3*, 170–188. [[CrossRef](#)]
54. Van Genuchten, M.T. A closed-form equation for predicting the hydraulic conductivity of unsaturated soils. *Soil Sci. Soc. Am. J.* **1980**, *5*, 892–898. [[CrossRef](#)]
55. Yi, Y.; Yang, D.; Huang, J.; Chen, D. Evaluation of MODIS surface reflectance products for wheat leaf area index (LAI) retrieval. *ISPRS J. Photogramm. Remote Sens.* **2008**, *6*, 661–677. [[CrossRef](#)]
56. Sun, T. *Retrieval of Crop Leaf Area Index: A Case Study of Paddy Rice and Wheat*; Nanjing University of Information Science and Technology: Nanjing, China, 2013. (In Chinese)
57. Fang, H.; Li, W.; Wei, S.; Jiang, C. Seasonal variation of leaf area index (LAI) over paddy rice fields in NE China: Intercomparison of destructive sampling, LAI-2200, digital hemispherical photography (DHP), and AccuPAR methods. *Agric. For. Meteorol.* **2014**, *198*, 126–141. [[CrossRef](#)]
58. Sun, Z. *The Study of Productivity and Carbon Storage Estimation in the Southern of China’s Grasslands*; Nanjing University: Nanjing, China, 2012. (In Chinese)
59. Wang, J.; Li, F.; Yi, J. The Forecasting and Regulation Hydraulic Model of Qinhuai River Catchment. *Sciencepaper*. Available online: <http://www.paper.edu.cn> (accessed on 6 October 2006). (In Chinese).
60. Hijmans, R.J.; Cameron, S.E.; Parra, J.L.; Jones, P.G.; Jarvis, A. Very high resolution interpolated climate surfaces for global land areas. *Int. J. Climatol.* **2005**, *15*, 1965–1978. [[CrossRef](#)]
61. Refsgaard, J.C. Parameterisation, calibration and validation of distributed hydrological models. *J. Hydrol.* **1997**, *1–4*, 69–97. [[CrossRef](#)]

62. Wilson, K.; Goldstein, A.; Falge, E.; Aubinet, M.; Baldocchi, D.; Berbigier, P.; Bernhofer, C.; Ceulemans, R.; Han, D.; Field, C. Energy balance closure at FLUXNET sites. *Agric. For. Meteorol.* **2002**, *1*, 223–243. [[CrossRef](#)]
63. Ma, Q. *Research on Drought Assessment and Forecast in Huanghui Basin Based on MIKE SHE.*; Northwest A & F University: Yanglin, China, 2014. (In Chinese)
64. Mann, H.B. Nonparametric Tests against Trend. *Econometrica* **1945**, *3*, 245–259. [[CrossRef](#)]
65. Kendall, M.G. Rank correlation methods. *Br. J. Psychol.* **1990**, *1*, 86–91. [[CrossRef](#)]
66. Hamed, K.H. Trend detection in hydrologic data: The Mann–Kendall trend test under the scaling hypothesis. *J. Hydrol.* **2008**, *3–4*, 350–363. [[CrossRef](#)]
67. Litvak, E.; Manago, K.; Hogue, T.; Pataki, D. Evapotranspiration of urban landscapes in Los Angeles, California at the municipal scale. *Water Resour. Res.* **2017**, *53*, 4236–4252. [[CrossRef](#)]
68. Grimmond, C.; Oke, T. Evapotranspiration rates in urban areas. *IAHS Publ.* **1999**, *259*, 235–244.
69. Hao, L.; Huang, X.; Qin, M.; Liu, Y.; Li, W.; Sun, G. Ecohydrological processes explain urban dry island effects in a wet region, southern China. *Water Resour. Res.* **2018**, *9*, 6757–6771. [[CrossRef](#)]
70. Locatelli, L.; Mark, O.; Mikkelsen, P.S.; Arnbjerg-Nielsen, K.; Deletic, A.; Roldin, M.; Binning, P.J. Hydrologic impact of urbanization with extensive stormwater infiltration. *J. Hydrol.* **2017**, *544*, 524–537. [[CrossRef](#)]
71. Chen, J.; Xiubin, L.I. Simulation of hydrological response to land-cover changes. *Chin. J. Appl. Ecol.* **2004**, *5*, 833.
72. Zhou, W.; Pan, J.; Liu, G. Analysis of Ecological Vegetation in Nanjing City. *Remote Sens. Technol. Appl.* **2002**, *1*, 22–26.
73. Yan, Z.; Wang, S.; Ma, D.; Liu, B.; Lin, H.; Li, S. Meteorological Factors Affecting Pan Evaporation in the Haihe River Basin, China. *Water* **2019**, *11*, 317. [[CrossRef](#)]
74. Wang, K.; Dickinson, R.E. A review of global terrestrial evapotranspiration: Observation, modeling, climatology, and climatic variability. *Rev. Geophys.* **2012**, *50*, 2. [[CrossRef](#)]
75. Goyal, R.K. Sensitivity of evapotranspiration to global warming: A case study of arid zone of Rajasthan (India). *Agric. Water Manag.* **2004**, *1*, 1–11. [[CrossRef](#)]
76. Ni, G.; Sun, F.; Yang, D.; Cong, Z.; Lei, Z. Analysis of actual evaporation variability over China during the last half century using the Budyko hypothesis. *IAHS-AISH Publ.* **2007**, *311*, 465–472.
77. Gao, G.; Xu, C.; Chen, D.; Singh, V. Spatial and temporal characteristics of actual evapotranspiration over Haihe River basin in China. *Stoch. Environ. Res. Risk Assess.* **2012**, *5*, 655–669. [[CrossRef](#)]
78. Liu, M.; Hu, D. Response of Wetland Evapotranspiration to Land Use/Cover Change and Climate Change in Liaohe River Delta, China. *Water* **2019**, *11*, 955. [[CrossRef](#)]
79. Jung, M.; Reichstein, M.; Ciais, P.; Seneviratne, S.I.; Sheffield, J.; Goulden, M.L.; Bonan, G.; Cescatti, A.; Chen, J.; De Jeu, R. Recent decline in the global land evapotranspiration trend due to limited moisture supply. *Nature* **2010**, *7318*, 951. [[CrossRef](#)]
80. Nayak, A.K.; Shahid, M.; Nayak, A.D.; Dhal, B.; Moharana, K.C.; Mondal, B.; Tripathi, R.; Mohapatra, S.D.; Bhattacharyya, P.; Jambhulkar, N.N. Assessment of ecosystem services of rice farms in eastern India. *Ecol. Process.* **2019**, *1*, 35. [[CrossRef](#)]
81. Batchelor, C.; Roberts, J. Evaporation from the irrigation water, foliage and panicles of paddy rice in north-east Sri Lanka. *Agric. Meteorol.* **1983**, *1*, 11–26. [[CrossRef](#)]
82. Hao, Z.; Zhao, H.; Zhang, C.; Zhou, H.; Zhao, H.; Wang, H. Correlation Analysis Between Groundwater Decline Trend and Human-Induced Factors in Bashang Region. *Water* **2019**, *11*, 473. [[CrossRef](#)]
83. Olchev, A.; Ibrom, A.; Priess, J.; Erasmi, S.; Leemhuis, C.; Twele, A.; Radler, K.; Kreilein, H.; Panferov, O.; Gravenhorst, G. Effects of land-use changes on evapotranspiration of tropical rain forest margin area in Central Sulawesi (Indonesia): Modelling study with a regional SVAT model. *Ecol. Model.* **2008**, *1–2*, 131–137. [[CrossRef](#)]
84. Dietz, M.E.; Clausen, J.C. Stormwater runoff and export changes with development in a traditional and low impact subdivision. *J. Environ. Manag.* **2008**, *4*, 560–566. [[CrossRef](#)] [[PubMed](#)]
85. Im, S.; Brannan, K.M.; Mostaghimi, S. Simulating hydrologic and water quality impacts in an urbanizing watershed. *J. Am. Water Resour. Assoc.* **2003**, *6*, 1465–1479. [[CrossRef](#)]
86. Franczyk, J.; Chang, H. The effects of climate change and urbanization on the runoff of the Rock Creek basin in the Portland metropolitan area, Oregon, USA. *Hydrol. Process. Int. J.* **2009**, *6*, 805–815. [[CrossRef](#)]

87. Lee, J.E.; Lintner, B.R.; Neelin, J.D.; Jiang, X.; Gentine, P.; Boyce, C.K.; Fisher, J.B.; Perron, J.T.; Kubar, T.L.; Lee, J. Reduction of tropical land region precipitation variability via transpiration. *Geophys. Res. Lett.* **2012**, *19*, 279–289. [[CrossRef](#)]
88. Zhang, C. Madden—Julian Oscillation. *Rev. Geophys.* **2005**, *43*, RG2003. [[CrossRef](#)]
89. Wang-Erlandsson, L.; van der Ent, R.J.; Gordon, L.J.; Savenije, H.H.G. Contrasting roles of interception and transpiration in the hydrological cycle—Part 1: Temporal characteristics over land. *Earth Syst. Dyn.* **2014**, *2*, 441–469. [[CrossRef](#)]
90. Van der Ent, R.J.; Wang-Erlandsson, L.; Keys, P.W.; Savenije, H.H.G. Contrasting roles of interception and transpiration in the hydrological cycle—Part 2: Moisture recycling. *Earth Syst. Dyn.* **2014**, *5*, 471–489. [[CrossRef](#)]
91. Savenije, H.H.G. The importance of interception and why we should delete the term evapotranspiration from our vocabulary. *Hydrol. Process.* **2004**, *8*, 1507–1511. [[CrossRef](#)]
92. Bagley, J.E.; Desai, A.R.; Dirmeyer, P.A.; Foley, J.A. Effects of land cover change on moisture availability and potential crop yield in the world’s breadbaskets. *Environ. Res. Lett.* **2012**, *1*, 014009. [[CrossRef](#)]
93. Liang, M.; He, C.; Bian, H.; Sheng, L. MIKE SHE modeling of ecohydrological processes: Merits, applications, and challenges. *Ecol. Eng.* **2016**, *96*, 137–149.
94. Sahoo, G.; Ray, C.; De Carlo, E. Calibration and validation of a physically distributed hydrological model, MIKE SHE, to predict streamflow at high frequency in a flashy mountainous Hawaii stream. *J. Hydrol.* **2006**, *327*, 94–109. [[CrossRef](#)]



© 2020 by the authors. Licensee MDPI, Basel, Switzerland. This article is an open access article distributed under the terms and conditions of the Creative Commons Attribution (CC BY) license (<http://creativecommons.org/licenses/by/4.0/>).